ECHO: Empirical Characterization and Height Optimization of UAV-to-Underground Channels

Syed Muhammad Hashir[1], Mehmet C. Vuran[2], and Joseph Camp[1]
[1]Department of Electrical and Computer Engineering, Southern Methodist University, Dallas, TX, USA
[2]School of Computing, University of Nebraska-Lincoln, Lincoln, NE, USA
Email: {hashirs, camp}@smu.edu, mcv@unl.edu

***Abstract*—This paper explores the nexus of two emerging Internet of Things (IoT) components in precision agriculture, which requires vast amounts of agriculture fields to be monitored from air and soil for food production with efficient resource utilization. On the one hand, unmanned aerial vehicles (UAVs) have gained interest in agricultural aerial inspection due to their ubiquity and observation scale. On the other hand, agricultural IoT devices, including buried soil sensors, have gained interest in improving natural resource efficiency in crop production. In this work, the path loss and fading characteristics in wireless links between a UAV and underground (UG) nodes (Air2UG link) are studied to design a UAV altitude optimization solution. A path loss model is developed for the Air2UG link, including fading in the channel, where fading is modeled using a Rician distribution and validated using the Kolmogorov-Smirnov test. Moreover, Rician-K is found to be dependent on the UAV altitude, which is modeled with a Gaussian function with an RMSE of $0.4 - 1.3$ dB. Furthermore, a novel altitude optimization solution is presented to minimize the bit error rate (BER). Results show that the lowest possible altitude does not always minimize the BER. Optimizing the altitude reduces the Air2UG link BER by as much as 8.6-fold. Likewise, altitude optimization can minimize the impacts of increasing burial depth on the BER. Our results and analysis are the first in this field and can be exploited to optimize the altitude and resources of a UAV node to communicate with the sensors embedded in the soil efficiently.**

***Index Terms*—UAV, underground Communication, software-defined radios, wireless underground sensor networks, precision agriculture.**

I. Introduction

Recently, the Internet of Underground Things (IoUT) field, which includes buried sensors and communication elements that communicate through the soil, has become important in various areas, including precision agriculture and environment monitoring [1]–[3], including commercial Ag-IoT products that provide real-time soil moisture and temperature sensing [4]–[6]. IoUT devices are expected to operate in the different underground (UG) environments which comprise various soil mediums, tunnels, and UG mines [7]–[9]. However, in the majority of IoUT deployments, connectivity infrastructure is limited. Unmanned aerial vehicles (UAVs) can be utilized in IoUT to acquire data from the UG sensor nodes without needing a vertical infrastructure [10], [11]. This approach may help reduce power consumption, signal interference, and data collection time. However, the radio propagation characteristics of air-to-underground (Air2UG) channels are not well known.

For a buried UG device, there are two relevant link types: *(i) UG2UG link* when two nodes are buried in the UG medium and *(ii) UG2AG (uplink)/AG2UG (downlink)* when one of the nodes is above ground (AG), and other is buried. Propagation characteristics of UG2UG and UG2AG links have been characterized separately. In [12], the UG2UG link in a soil medium was modeled as a three-wave, closed-form UG channel and validated through testbed experiments. The channel models of UG2AG and AG2UG links were developed in [13], [14] and supported by empirical measurements in an IoUT testbed. In [15], the UG soil medium was considered to model the statistical propagation characteristics of both UG2UG and UG2AG links, where antennas were buried in the soil, and measurements were taken between the antennas, showing dependence on the soil type, soil moisture, antenna depth, and transmission frequency, and the root mean square delay spread of the link followed a log-normal distribution.

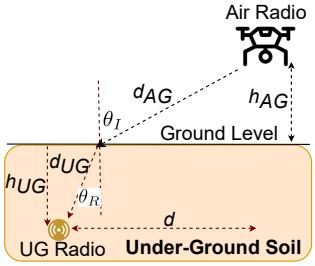

Fig. 1: Downlink channel between Air and UG radios

Researchers have also shown interest in using UG communication in Low Power Wide Area Networks (*e.g.*, LoRa). In [16], authors developed a LoRa-based testbed to study UG2UG and UG2AG links in four different soils. They found that the maximum transmission coverage in UG2UG and UG2AG links depended on the soil properties, varying between 4-20 m and 100-200 m, respectively. In [17], we considered LoRa for the UG2AG and AG2UG links. The dependency of LoRa performance on soil properties was studied. Further, the bit error rate (BER) of LoRa was formulated as a function of the soil parameters based on statistical UG channel models in [15], [18] and validated using measurements in an outdoor environment. It was also found that the antenna return loss changes with the burial depth [19]. The main challenge with IoUT is the relatively lower communication range because of the attenuation in the soil path. This leads to the need for local gateways [4], [5].

An alternative to deploying gateways in agricultural fields may be to utilize UAVs. UAVs have become very popular in providing Internet of Things (IoT) communication services. UAVs have numerous applications in wireless communication, such as communication relaying and broadband services [20]–[22]. In IoT, UAVs are utilized for data collection of ground sensors. For example, we considered a wireless-powered communication network [23], where a UAV was deployed to serve wireless-powered sensors on the ground by transferring power in the downlink direction and collecting data in the uplink direction. UAVs are easily operable and highly maneuverable and could potentially be used with IoUT devices.

In this work, we consider a novel topology in UG communications where one of the nodes is placed on a UAV, and the other is placed in the UG medium (*i.e.*, **the Air2UG channel**). To the best of our knowledge, this is the first work that analyzes the Air2UG channel through extensive empirical evaluations. We study the wireless channel characteristics of the Air2UG link through outdoor UAV measurements in dynamic soil conditions. Accordingly, we develop a novel optimal UAV altitude management mechanism to minimize BER. The main contributions of this paper are as follows:

- We empirically study the in-field characteristics of the Air2UG channel by taking path loss measurements of UAV and UG nodes at multiple depths in the soil.
- We show that the path loss model of the AG2UG link developed in [18], [24] can be utilized to estimate the deterministic components of path loss in the Air2UG link with root-mean-squared error (RMSE) of $1.1-4.1$ dB.
- We show that the small-scale fading of the Air2UG channel follows a Rician distribution, and we validate our claim by using the confidence-based equality test. Accordingly, we develop a new Air2UG channel model by incorporating the channel fading characteristics in the path loss model.
- We show that the Rician-K parameter in the Air2UG link significantly varies with the UAV altitude at all soil depths and moisture levels. To this end, a Gaussian function can be used to model the variation with an RMSE of $0.4-1.3$ dB, which is essential in estimating the wireless performance at multiple UAV altitudes.
- We show that the lowest possible altitude does not always minimize BER. Accordingly, we develop a novel mechanism to optimize the UAV altitude, which minimizes the BER of DBPSK modulation in a Rician fading channel. This solution utilizes a Gaussian function to estimate the Rician-K parameter at multiple UAV altitudes. We present a closed-form solution and find the best altitude at the centroid of the Gaussian peak. Accordingly, optimizing the UAV altitude improves the BER by $4.1-8.6$-fold at $10-20$ cm soil depths, respectively.

The rest of the paper is organized as follows: In Section II, we describe the wireless channel model for UG communications and its dependency on soil properties. Section III details the experiment setup, measurement steps, and location-specific soil properties. Results and comparisons are presented in Section IV. The Air2UG channel model and the UAV altitude optimization mechanism are detailed in Section V. Finally, Section VI concludes the paper.

II. Background

In this section, we present the UG channel characteristics in the soil medium and the relevant propagation model.

A. Air to Underground Path Loss Model and Link Budget

The downlink communication channel between air and UG nodes is shown in Fig 1. The path loss model of a similar link with an above-ground (AG) node was developed in [13], [14], [18], [24]. The communication link comprises two path components: the UG propagation component in the soil medium and the AG component in the air. The RF propagation path losses associated with those components are the path loss in the soil medium (PL_{UG}), the path loss in the air medium (PL_{OTA}), and the refraction loss due to the air-soil interface (PL_R).[1] The total path loss can be written as:

$$PL[dB] = PL_{UG}(d_{UG}) + PL_{OTA}(d_{AG}) + PL_R, \quad (1)$$

where d_{UG} is the length of the underground signal path between the ground surface and the UG node, d_{AG} is the length of the over-the-air signal path between the ground surface and the Air/AG node as depicted in Fig. 1, and PL_R is the refraction loss at the air-soil interface. The different path loss terms in (1) are defined as follows:

$$PL_{UG}(d_{UG}) = 6.4 + 20\log(d_{UG}) + 20\log(\beta) + 8.69\alpha d_{UG}, \quad (2)$$

$$PL_{OTA}(d_{AG}) = -147.6 + 10\eta\log(d_{AG}) + 20\log(f), \quad (3)$$

$$PL_R = 10\log\frac{\left(\cos\theta_I + \sqrt{\epsilon_s^{'} - \sin^2(\theta_I)}\right)^2}{4\cos\theta_I\sqrt{\epsilon_s^{'} - \sin^2(\theta_I)}}, \quad (4)$$

where α and β correspond to the attenuation and phase shift of the wave in soil, respectively, η is the AG attenuation coefficient which varies between 2.8 and 3.3 due to attenuation and reflections [25], f is the carrier frequency of the propagating signal, $\epsilon_s^{'}$ is the real part of the relative dielectric constant of the soil-water mixture and θ_I is the angle of incidence from Snell's law.

The signal propagation in the soil medium is mostly affected by the permittivity of the soil, which is dependent on the soil properties including moisture, textural composition, and bulk density [12]. Therefore, it is important to characterize the impacts of the permittivity of soil on wireless propagation. The complex-valued permittivity of the soil can be defined as $\epsilon_s = \epsilon_s^{'} - \iota\epsilon_s^{''}$, where $\epsilon_s^{'}$ and $\epsilon_s^{''}$ are the real and imaginary parts of relative permittivity of the soil. For the frequency range

[1]Note that the refraction loss PL_R of uplink and downlink communication directions are defined separately and can not be interchanged [13], [18], [24].

of 300-1300 MHz, $\epsilon_s^{'}$ and $\epsilon_s^{''}$ are experimentally characterized as [26]:

$$\epsilon_s^{'} = 1.15\left[1 + \frac{\rho_b}{\rho_s}\left(\epsilon_m^{\delta} - 1\right) + (m_v)^{v^{'}}(\epsilon_{fw}^{'})^{\delta} - m_v\right]^{\frac{1}{\delta}} - 0.68, \tag{5}$$

$$\epsilon_s^{''} = \left[(m_v)^{v^{''}}(\epsilon_{fw}^{''})^{\delta}\right]^{\frac{1}{\delta}}, \tag{6}$$

where ρ_s and ρ_b correspond to the particle density and bulk density of the soil, respectively. ϵ_m is the dielectric constant of the soil solids and is defined as $\epsilon_m = (1.01 + 0.44\rho_s)^2 - 0.062$, m_v is the volumetric moisture content, $\delta = 0.65$ is the empirically determined constant, $v^{'}$ and $v^{''}$ are the soil dependent constants which are also determined empirically and defined as $v^{'} = 1.2748 - 0.519S - 0.152C$ and $v^{''} = 1.33797 - 0.603S - 0.166C$, where C and S are the mass fractions of clay and sand in the soil mixture, respectively. The quantities $\epsilon_{fw}^{'}$, and $\epsilon_{fw}^{''}$ are the real and imaginary parts of the dielectric constant of water which are explained in [9], [24], [26]. Moreover, the complex propagation constant γ of the electromagnetic wave in the soil is defined as $\gamma = \beta + \iota\alpha$, where α and β can be found as:

$$\alpha = \omega\sqrt{\frac{\mu\epsilon_s^{'}}{2}\left[\sqrt{1 + \left(\frac{\epsilon_s^{''}}{\epsilon_s^{'}}\right)^2} - 1\right]}, \tag{7}$$

$$\beta = \omega\sqrt{\frac{\mu\epsilon_s^{'}}{2}\left[\sqrt{1 + \left(\frac{\epsilon_s^{''}}{\epsilon_s^{'}}\right)^2} + 1\right]}, \tag{8}$$

where ω is the angular velocity and μ is the magnetic permeability of the soil. Based on the path loss in (1), the link budget is given by [25]:

$$P_{RX} = P_{TX} + G_{RX} + G_{TX} + 10\log_{10}\left(1 - 10^{-\frac{RL}{10}}\right) - PL, \tag{9}$$

where P_{TX} and P_{RX} are the transmit and received power of the signal, G_{TX} and G_{RX} are the transmitter and receiver antenna gains, respectively, and RL is the return loss of the antenna in the UG soil medium. It is well known that the return loss of the antenna changes when buried in the soil [19]. In this paper, we utilize a patented wide-band antenna in the soil medium [27]. Moreover, we utilize the model in (1) to estimate the path loss in the Air2UG downlink channel.[2] We only consider the downlink channel in this work, but we also aim to study the uplink channel in the future.

III. Experiment Setup

We first present the software-defined radio (SDR)-based measurement system which we utilize to take the outdoor measurements, followed by the details of the measurement setup and area-specific soil properties.

[2]Note that the Air2UG channel in this work observes higher vertical distance through aerial platform compared to the AG2UG channel in [13], [18].

TABLE I: Measurement system parameters

Parameter	Value
Carrier Frequency	1.241 GHz
TX Power	15.5 dBm
Sampling rate	300K samples/seconds
TX Antenna	Tri-band (SMA-703)
RX Antenna	Custom wide-band
Transmit signal	Sine wave
Radiation pattern	Omni Directional
UAV	DJI Matrice 300 RTK

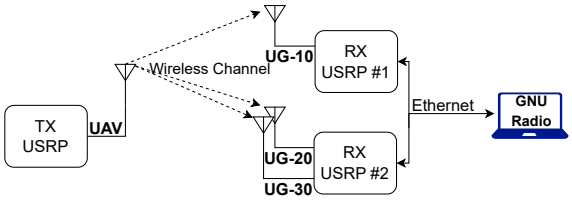

Fig. 2: Measurement system setup

A. Measurement System

We utilize USRP E312 SDRs [28] on both transmitter and receiver to take path loss measurements. USRP E312 can work in two different modes: *(i)* embedded mode: when the USRP can operate standalone to transmit and receive the In-Phase and Quadrature (IQ) samples and does not require any external connection, and *(ii)* network mode: when the USRP needs a host machine for command and control. We utilize both modes of the USRP in this work and design a system that comprises three USRP E312 as depicted in Fig. 2. We mount one of the USRPs on the commercial UAV as shown in Fig. 3b (top), which operates in standalone mode to transmit a continuous sinusoidal signal at a particular carrier frequency. The other two USRPs work in network mode using a single host PC to capture the transmitted signal at three buried receiver antennas. Note that each USRP E312 has two RF chains that can simultaneously capture the signal. Further, we utilize the GNU Radio flowgraph at the receiver to record received signal samples which are post-processed in MATLAB to generate results. Also, we employ an omnidirectional antenna on the UAV which is useful to communicate with a large number of UG sensor nodes in the field with limited sweeping. The rest of the measurement system parameters are listed in Table I.

B. Measurement Plan

We are interested in measuring the path loss to characterize the channel and check the validity of the path loss model described in Section II-A on the Air2UG link. For this purpose, the measurements are taken in the topology which is shown in Fig. 3a, where three antennas are buried in the soil at 10, 20, and 30 cm depths. The depths are chosen to represent the typical soil moisture sensor deployments, which capture the root zone of a crop. All the receiver antennas are connected with USRPs through 50 cm long cables, and the horizontal separation between each antenna is 50 cm. The UAV flies directly above the antenna at the 20 cm depth and changes its altitude between 5 and 26 meters. The UAV hovers every 3 meters for 20 seconds through an automated flight plan. Since

the transmitter is set to continuous transmission, the transmitted signal data is captured at all receiver antennas during the hover time of the UAV. The aerial view of the measurement site is given in Fig. 3b (bottom). The measurement location is enclosed in a wooden fort structure with an open interior courtyard and high trees in the vicinity.

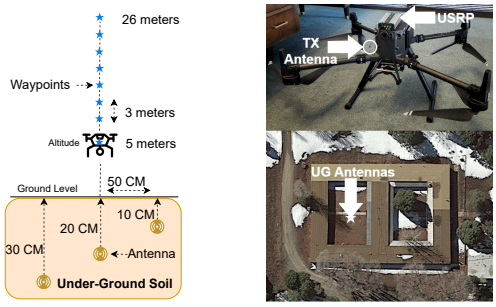

(a) (b)

Fig. 3: (a) Measurement topology, (b) UAV-based SDR platform (Top), Aerial view of the site (Bottom)

For soil moisture measurements, three Watermark moisture sensors [29] are buried side by side with the UG antennas. The measured soil moisture sensor values reflect soil water tension in centibars (cB), which is inversely proportional to soil moisture. All the communication measurements are taken at two different soil moisture levels with measured soil water tension values of 0 centibars (cB) (saturated wet soil) and 8 cB (dry soil). To achieve different moisture levels, first, the soil is saturated with water, followed by wet soil experiments. Then, after the moisture level changes from 0 to 8 cB, the dry soil experiments are performed.

C. Soil Properties

The soil texture at the measurement location is sandy clay loam at all depths. The soil's bulk density and the textural composition (sand, silt, and clay percentages) marginally vary with depth. At 10 cm, the percentages of sand, silt, and clay contents in the soil are 56, 23, and 21, respectively. Similarly, at 20 cm, the percentages are 56, 20, and 24, and at 30 cm, the percentages are 59, 17, and 24. The bulk density values at 10, 20, and 30 cm depths are 0.58, 0.89, and 0.70 gr/cm^3, respectively.

IV. Infield Characterization of the Air2UG Channel

In this section, we present our results by post-processing the received IQ data which includes calculating the received signal magnitude and path loss at all the receiver antennas. We also analyze the return loss of the wide-band antenna. The results are given as follows.

A. Antenna Return Loss

The return loss of the wide-band antenna, as shown in Fig. 4, is measured using a vector network analyzer in the AG and UG settings. The return loss of the transmitter antenna which is mounted on the UAV is also shown in Fig. 4. Since 10 dB return loss corresponds to 90% of the transmitted power. We consider a return loss of -10 dB as a threshold to compare the results at all frequencies. It can be seen that the return loss of the wide-band antenna significantly changes in the UG soil compared to the AG. For instance, the return loss at 0.1 GHz in the AG is significantly higher than the -10 dB while in the UG, the return loss is lower than the -10 dB at all depths which infers that the 0.1 GHz frequency can be utilized for transmission in UG. Contrary, the return loss at 0.58 GHz in the AG is lower than the -10 dB threshold while in the UG, the return loss is above the -10 dB threshold at all depths. Following, at the transmission frequency 1.241 GHz, the return loss of the wide-band antenna in the UG is lower than -10 dB at 10 cm, and 20 cm depths while at 30 cm, the return loss is almost equal to the -10 dB. Similarly, the return loss of the TX antenna mounted on the UAV is significantly lower than -10 dB at the transmission frequency which infers that the TX antenna is suitable to communicate with the wide-band antenna buried in the UG. Moreover, the impact of soil moisture on the return loss of wide-band antenna in the UG can be found in [30].

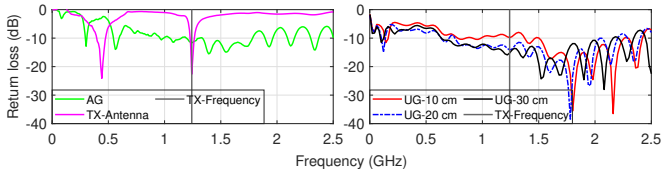

Fig. 4: Return loss of the TX antenna mounted on UAV, and the custom wide-band antenna placed at AG and UG.

B. Air2UG Channel Path Loss

The measured path loss values are calculated for measurement topology using the received IQ samples. The path loss results at all UG antennas for the measurement topology are shown in Fig. 5. It can be seen that the path loss increases with the increase in direct distance between UG antennas and UAV at all antenna depths. At 8 cB (dry soil), the path loss increases by 5.9 dB and 17.6 dB on average when the antenna depth changes from 10 cm to 20 cm and 20 cm to 30 cm, respectively. The path loss variation at 0 cB (wet soil), and 10-20 cm antenna depth is very similar to that of 8 cB results while at 30 cm, the path loss values show that the received signal is lost after 5 m altitude. The increase in soil moisture shows that the path loss increases by 3.0 dB, and 4.5 dB at 10 cm, and 20 cm depths, respectively. Also, note that the fading in the path loss (error bars) is not consistent with the altitude, and the highest fading is found at 26 m altitude.

Next, the path loss is estimated at 10-30 cm antenna depths using the path loss model in Section II-A. The estimated path loss results are also shown in Fig. 5, while the measurement area-specific soil parameters used in the model are listed in Table II. It is found that the path loss model fits our results well and the RMSE values between the estimated and measured results at 10 cm and 20 cm depths, and soil moisture 0 cB are

3.8 dB and 1.6 dB, respectively. Similarly, at 8 cB, RMSE values are 4.1 dB, and 1.1 dB. For the 30 cm depth, we estimated the path loss at only 8 cB and the RMSE value is 2.8 dB. Also, it is found that the UG 30 cm antenna has a very high penetration loss and low signal-to-noise ratio which becomes more severe with the increase in soil moisture. Therefore, we do not include the results at 30 cm soil depth in the further analysis. The comparison between measured and estimated results shows that the AG2UG link model can be utilized to model the path loss in the Air2UG channel.

TABLE II: Soil parameters

Parameter	Value
$\rho_s(gr/cm^3)$	2.65 [31]
$\rho_b(gr/cm^3)$	0.58 (10 cm), 0.89 (20 cm), 0.70 (30 cm)
m_v	0.35 [32], [33]
S	0.56 (10, 20 cm), 0.59 (30 cm)
C	0.21 (10 cm), 0.24 (20, 30 cm)
ϵ_o, $\epsilon_{fw}^{'}$, μ, ϵ_{w0}, $\epsilon_{w\infty}$	55.26 [17], 79.71, 6 [34], 80.1 [33], 4.9 [33]
$\epsilon_{fw}^{''}$	25.31 (10 cm), 40.27 (20 cm), 31.81 (30 cm)
δ_{eff}	0.08 (10 cm), 0.17 (20 cm), 0.11 (30 cm)
$2\pi\tau_w(s)$	0.58×10^{-10} [33]

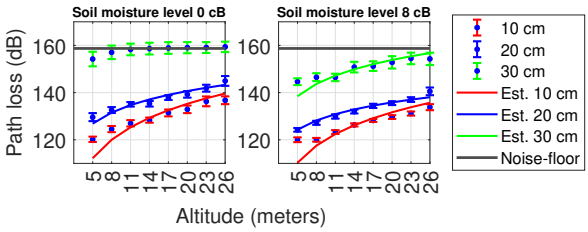

Fig. 5: Path loss at multiple altitudes, antenna depths, and soil moisture levels.

C. Small-scale fading

The received signal magnitude results are utilized to model fading in the Air2UG channel. We model small-scale fading in our measurements with a Rician distribution due to the line of sight scenario between the UAV and ground path. For each waypoint, the Rician distribution function is fitted on the measured signal using the maximum likelihood estimation. As a result, the Rician distribution parameters (i.e., non-centrality (s) and scale (σ)) are generated. Furthermore, the Rician-K value is calculated, which is defined as the ratio between the power in the direct radio propagation path and the reflected or scattered paths (i.e., $K = s^2/2\sigma^2$).

For measurement topology (Fig. 3a), the Rician-K values at soil moisture levels 0 cB and 8 cB are shown in Fig. 6a. It can be seen that in all cases, the Rician-K value first increases and then decreases with the altitude of the UAV. The increase in soil moisture decreases the Rician-K value by 4.3 dB and 2.4 dB (on average) at the depths of 10 cm and 20 cm, respectively. At 8 cB, the antenna at a depth of 10 cm performs better overall. On the other hand at 0 cB, the 20 cm-depth antenna has performance gains over the 10 cm-depth antenna at most altitudes. The reasons for the performance gain of the 20 cm-depth antenna are the better return loss at the transmission frequency and the variation of soil properties from 10 to 20 cm depth. Note that Rician distribution can be approximated

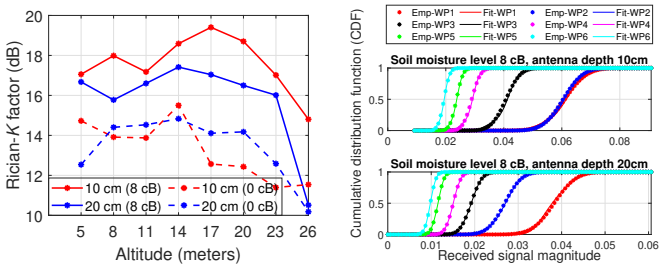

Fig. 6: Results at multiple altitudes/waypoints (WP), soil depths, and moisture levels (a) Rician-K, (b) Empirical CDF of the received signal magnitude (emp), and corresponding fitted Rician CDF (fit).

by a Gaussian when $K >> 1$.[3] Gaussian is a much simpler distribution than Rician.

Last, the two-sample K-S test is performed on the results to check the goodness-of-fit of the proposed fading distribution on the measured results. The two-sample K-S test is an equality test that is useful for testing whether the two observed sets of samples are from the same distribution. Therefore, the empirical CDF of the measured data and the CDF of the respective fitted Rician distribution are calculated, and the K-S test is performed on all the waypoints in the measurement topology. The empirical CDF of the received signal magnitude and corresponding fitted Rician CDF at waypoints 1-6 (5-20 m altitudes) in measurement topology are shown in Fig. 6b. It can be seen that the fitted Rician CDF follows the empirical CDF at all waypoints with an error less than 10^{-10}. It is also found that the K-S test is passed at all the waypoints with a 10% significance level which shows that the small-scale fading in the Air2UG link follows Rician distribution and it can be utilized to predict wireless communication performance in the Air2UG link.

V. Proposed Model and Altitude Optimization

In this section, we utilized the findings in the previous section to develop new models. More specifically, we present a path loss model for the Air2UG channel, fading distribution variation model as a function of UAV altitude, and a novel optimal UAV altitude mechanism while minimizing the BER performance.

A. Air2UG Path Loss and Fading Distribution Model

We found that the path loss in the Air2UG channel follows the model in (1) and the fading in the received signal follows a Rician distribution. Therefore, we present a model for path loss in the Air2UG channel (downlink) which is defined as

$$PL[dB] = PL_{UG}(d_{UG}) + PL_{OTA}(d_{AG}) + PL_R + \kappa\,, \quad (10)$$

[3]We observed elevated Rician-K values which will be further investigated in future work.

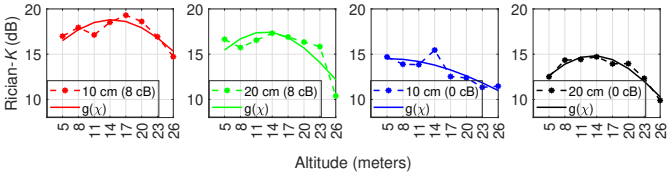

Fig. 7: Fitted Gaussian function $g(\chi)$ and empirical Rician-K at multiple soil depth, moisture, and UAV altitudes.

where κ is a random variable that follows a Rician distribution, and $PL_{UG}(d_{UG})$, $PL_{OTA}(d_{AG})$,[4] and PL_R are defined in (2)-(4), respectively.

As shown in Fig. 6a, the Rician-K value of the Air2UG channel changes with the UAV altitude. Next, we show that the Rician-K value can be captured by a Gaussian function as a function of the UAV altitude. More specifically, the Gaussian function with altitude, χ, can be defined as:

$$g(\chi) = a \exp\left(- \frac{(\chi - b)^2}{2c^2} \right) , \tag{11}$$

where a, b, and c are the amplitude, centroid, and width of the Gaussian peak, respectively. Following, we fitted the Gaussian function on the Rician-K values in Fig. 6a. The results are shown in Fig. 7. It can be seen that the Gaussian function captures the estimated Rician-K values well at all soil depths and moisture values. The RMSE ranges between 0.4-1.3 dB, where the highest error is mostly found at the maximum value of the Rician-K across all altitudes. The set of fitted Gaussian function parameters {a, b, c} at 10 cm soil depth are {14.5, 5.1, 39.5} at 0 cB moisture level, and {18.8, 14.3, 25.7} at 8 cB moisture level. Similarly, at 20 cm, the set of fitted Gaussian function parameters are {14.8, 13.3, 20.8} at 0 cB, and {17.4, 12.7, 22.1} at 8 cB. It is observed that the {a, b, c} values vary with soil depth and moisture values. Also, the peak value of the Gaussian peak is significantly reduced by the soil moisture compared to soil depth. We can conclude that the Gaussian function can be used to estimate Rician-K values at all UAV altitudes.

B. UAV Altitude Optimization

We present a novel UAV altitude optimization mechanism to minimize the BER of the Air2UG link. Usually, the communication rate requirement in an IoT network is limited. Therefore, we utilize the BER expression of DBPSK modulation in the Rician fading channel given in [35] as a performance metric to optimize the UAV altitude. The BER as a function of UAV altitude in the Rician fading channel for DBPSK modulation can be written as:

$$P_b(\chi) = \frac{\left(1 + \hat{K}(\chi)\right)}{2\left(1 + \hat{K}(\chi) + \overline{\gamma}(\chi)\right)} \exp\left[- \frac{\hat{K}(\chi)\overline{\gamma}(\chi)}{1 + \hat{K}(\chi) + \overline{\gamma}(\chi)} \right] , \tag{12}$$

where $\overline{\gamma}(x)$ is the average SNR for the Rician fading distribution channel and is defined as $\overline{\gamma}(\chi) = (1 + \hat{K}(\chi))2\sigma^2 E_b/N_0$,

[4]The OTA distance in our experiment correspond to the vertical distance.

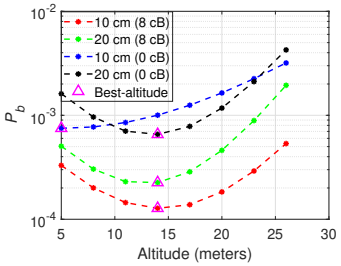

Fig. 8: BER with $\lambda = 35$

$\hat{K}(\chi)$ is the estimated value of Rician-K parameter using the Gaussian model in (11), i.e., $\hat{K}(\chi) = g(\chi)$, and altitude χ is the same vertical distance as the d_{AG} in (10). The altitude optimization problem to minimize the BER can be written as:

$$\min_{\chi} \;\; P_b(\chi) \tag{13a}$$

$$s.t. \quad C1 : \lambda_{\min} \leq \lambda \; , \; C2 : \chi_{\min} \leq \chi \leq \chi_{\max} \; ,$$

where $\lambda = \frac{E_b}{N_0}$, $\lambda_{\min}$ corresponds to the minimum signal-to-noise ratio per bit required for reliable communication, and $\chi_{\min}$ and $\chi_{\max}$ are the minimum and maximum altitude for the safe operation of the UAV, respectively. The objective function (13a) is convex with respect to the UAV altitude, χ, where $\frac{d^2}{d\chi^2} P_b(\chi) > 0, \forall \chi > 0$. Therefore, problem (13) can be solved by taking the first order derivative of the objective function (13a) with respect to χ i.e., $\frac{d}{d\chi} P_b(\chi) = 0$ and finding the close form solution for the χ. Moreover, to satisfy the constraint $C1$, we assume minimal signal-to-noise ratio per bit for transmission in (13a) i.e., $\lambda = \lambda_{\min}$. By solving $\frac{d}{d\chi} P_b(\chi) = 0$ to find χ, we found that $\chi = b$ which means that the optimum altitude of UAV is found at the centroid of the Gaussian peak and to satisfy the constraint $C2$, the final optimal solution can be written as:

$$\chi^* = \min\{\max\{b, \chi_{\min}\}, \chi_{\max}\} \; . \tag{14}$$

Fig. 8 shows the BER calculated for different UAV altitudes at multiple antenna depths and moisture values. An important observation is that the lowest possible altitude does not minimize the BER, P_b, which first decreases and then increases with the altitude. Accordingly, the best altitude in Fig. 8 is calculated using the solution of the proposed optimization problem given in (14), where we assume $\chi_{\min} = 5$ and $\chi_{\max} = 25$. The best altitude varies with the soil depth and moisture values. At 0 cB (wet soil), by optimizing the UAV altitude, similar bit-level performance can be achieved for antennas buried at different soil depths. Accordingly, UAV altitude optimization minimizes the impacts of increasing burial depth. This allows for better root monitoring capabilities with deeper soil moisture sensor deployments. Moreover, by utilizing the proposed solution in (14) to optimize the UAV altitude, the BER at 10 cm soil depth improves by $4.19 - 4.25$-fold (0 cB-8 cB), and at 20 cm, the BER improves by $6.49 - 8.61$-fold, when compared with worst performing altitude. Our results and findings can be utilized in the designing and deployment of Air-UG communication networks.

VI. Conclusion

In this paper, we study the wireless channel characteristics in the downlink between UAV and UG antennas buried at different soil depths. The impact of soil depth and moisture on the path loss and fading in the Air2UG link is shown through real outdoor measurements in the field. The derived path loss model of the AG2UG link is leveraged to estimate the path loss of the Air2UG link with minimal errors. The distribution of the measured fading is analyzed at UG antennas and it is shown that the small-scale fading in the Air2UG link follows Rician distribution which is verified through the K-S test. A new path loss model is proposed for the Air2UG link which includes the fading in the environment. Following this, the Rician-K parameter is calculated and analyzed at multiple UAV altitudes. It is shown that the Rician-K parameter depends on the UAV altitude and the Gaussian function can be used to estimate Rician-K at multiple UAV altitudes which is beneficial in estimating the wireless performance of the link. Moreover, a novel altitude optimization problem is proposed and solved which finds the best altitude of the UAV to provide significant performance improvement by minimizing the BER of DBPSK modulation with possible extension to other PSK modulation techniques. In the future, we plan to extend our analysis in this work for more soil types and moisture levels.

Acknowledgment

This work was supported by NSF grants CNS-1909381, ERC-2124376, CNS-2212050, and ECCS-2030272.

References

[1] P. Abouzar, D. G. Michelson, and M. Hamdi, "Rssi-based distributed self-localization for wireless sensor networks used in precision agriculture," *IEEE Trans. Wirel. Commun.*, vol. 15, no. 10, pp. 6638–6650, 2016.

[2] M. A. Akkaş, "Channel modeling of wireless sensor networks in oil," *Wireless Personal Communications*, vol. 95, no. 4, pp. 4337–4355, 2017.

[3] M. C. Vuran, A. Salam, R. Wong, and S. Irmak, "Internet of underground things in precision agriculture: Architecture and technology aspects," *Ad Hoc Networks*, vol. 81, pp. 160–173, dec 2018.

[4] "RealmV Furrow underground monitoring device," https://realmfive.com/product/agronomy/furrow-underground-monitoring-device/.

[5] "GroGru products," https://www.groguru.com/products/.

[6] "Soil Scout wireless soil moisture sensor," https://soilscout.com/solution/wireless-soil-moisture-sensor.

[7] Z. Sun, P. Wang, M. Vuran, M. Al-Rodhaan, A. Al-Dhelaan, and I. Akyildiz, "Mise-pipe: Magnetic induction-based wireless sensor networks for underground pipeline monitoring," *Ad Hoc Networks*, vol. 9, no. 3, pp. 218–227, 2011.

[8] M. A. Akkaş, I. F. Akyildiz, and R. Sokullu, "Terahertz channel modeling of underground sensor networks in oil reservoirs," in *2012 IEEE Glob. Commun. Conf.* IEEE, 2012, pp. 543–548.

[9] M. C. Vuran and I. F. Akyildiz, "Channel model and analysis for wireless underground sensor networks in soil medium," *Physical communication*, vol. 3, no. 4, pp. 245–254, 2010.

[10] S. Say, H. Inata, J. Liu, and S. Shimamoto, "Priority-based data gathering framework in uav-assisted wireless sensor networks," *IEEE Sensors Journal*, vol. 16, no. 14, pp. 5785–5794, 2016.

[11] M. Dong, K. Ota, M. Lin, Z. Tang, S. Du, and H. Zhu, "Uav-assisted data gathering in wireless sensor networks," *The Journal of Supercomputing*, vol. 70, no. 3, pp. 1142–1155, 2014.

[12] X. Dong and M. C. Vuran, "A channel model for wireless underground sensor networks using lateral waves," in *2011 IEEE Glob. Commun. Conf.* IEEE, 2011, pp. 1–6.

[13] A. Silva and M. Vuran, "Communication with aboveground devices in wireless underground sensor networks: An empirical study," in *IEEE Int. Conf. on Commun.*, 2010.

[14] X. Dong, M. C. Vuran, and S. Irmak, "Autonomous precision agriculture through integration of wireless underground sensor networks with center pivot irrigation systems," *Ad Hoc Networks*, vol. 11, no. 7, pp. 1975–1987, 2013.

[15] A. Salam, M. C. Vuran, and S. Irmak, "A statistical impulse response model based on empirical characterization of wireless underground channels," *IEEE Trans. Wirel. Commun.*, vol. 19, no. 9, pp. 5966–5981, 2020.

[16] M. Hardie and D. Hoyle, "Underground wireless data transmission using 433-mhz lora for agriculture," *Sensors*, vol. 19, no. 19, p. 4232, 2019.

[17] B. Zhou, V. S. S. L. Karanam, and M. C. Vuran, "Impacts of soil and antenna characteristics on lora in internet of underground things," in *2021 IEEE Glob. Commun. Conf.* IEEE, 2021, pp. 1–6.

[18] Z. Sun and I. F. Akyildiz, "Connectivity in wireless underground sensor networks," in *2010 7th Annual IEEE SECON*. IEEE, 2010, pp. 1–9.

[19] A. Salam, M. C. Vuran, X. Dong, C. Argyropoulos, and S. Irmak, "A theoretical model of underground dipole antennas for communications in internet of underground things," *IEEE Trans. Antennas Propag.*, vol. 67, no. 6, pp. 3996–4009, jun 2019.

[20] S. M. Hashir, S. Gupta, G. Megson, E. Aryafar, and J. Camp, "Rate maximization in a uav based full-duplex multi-user communication network using multi-objective optimization," *Electronics*, vol. 11, no. 3, p. 401, 2022.

[21] Y. Zeng, R. Zhang, and T. J. Lim, "Throughput maximization for mobile relaying systems," in *2016 IEEE Globecom Workshops*. IEEE, 2016, pp. 1–6.

[22] Q. Wu, J. Xu, Y. Zeng, D. W. K. Ng, N. Al-Dhahir, R. Schober, and A. L. Swindlehurst, "A comprehensive overview on 5g-and-beyond networks with uavs: From communications to sensing and intelligence," *IEEE Journal on Selected Areas in Communications*, vol. 39, no. 10, pp. 2912–2945, 2021.

[23] S. M. Hashir, A. Mehrabi, M. R. Mili, M. J. Emadi, D. W. K. Ng, and I. Krikidis, "Performance trade-off in uav-aided wireless-powered communication networks via multi-objective optimization," *IEEE Trans. Veh. Technol.*, vol. 70, no. 12, pp. 13 430–13 435, 2021.

[24] L. Li, M. C. Vuran, and I. F. Akyildiz, "Characteristics of underground channel for wireless underground sensor networks," in *Proc. Med-Hoc-Net*, vol. 7, 2007, pp. 13–15.

[25] X. Dong and M. C. Vuran, "Impacts of soil moisture on cognitive radio underground networks," in *2013 first international black sea conference on communications and networking (BlackSeaCom)*. IEEE, 2013, pp. 222–227.

[26] N. R. Peplinski, F. T. Ulaby, and M. C. Dobson, "Dielectric properties of soils in the 0.3-1.3-ghz range," *IEEE Trans. Geosci. Remote Sens.*, vol. 33, no. 3, pp. 803–807, 1995.

[27] M. C. Vuran, X. Dong, and D. Anthony, "Antenna for wireless underground communication," Grant US 9 532 118, Dec. 27, 2016.

[28] E. Research, 2022, accessed: 2022-09-30. [Online]. Available: https://www.ettus.com/about

[29] J. Chard, "Watermark soil moisture sensors: characteristics and operating instructions," *Utah State University*, 2002.

[30] A. Salam, M. C. Vuran, X. Dong, C. Argyropoulos, and S. Irmak, "A theoretical model of underground dipole antennas for communications in internet of underground things," *IEEE Trans. Antennas Propag.*, vol. 67, no. 6, pp. 3996–4009, 2019.

[31] S. Irmak, "Soil water content-and soil matric potential-based irrigation trigger values for different soil types," *Nebraska Extension NebGuide*, vol. 3045, 2019.

[32] S. Datta, S. Taghvaeian, J. Stivers *et al.*, "Understanding soil water content and thresholds for irrigation management," Oklahoma Cooperative Extension Service, Tech. Rep., 2017.

[33] A. Salam, M. C. Vuran, and S. Irmak, "Di-sense: In situ real-time permittivity estimation and soil moisture sensing using wireless underground communications," *Computer Networks*, vol. 151, pp. 31–41, 2019.

[34] L. W. Hacker and J. O. Carleton, "Soil survey of taos county and parts of rio arriba and mora counties, new mexico," 1982.

[35] P. Mahasukhon, M. Hempel, H. Sharif, T. Zhou, S. Ci, and H.-H. Chen, "Ber analysis of 802.11 b networks under mobility," in *2007 IEEE Int. Conf. on Commun.* IEEE, 2007, pp. 4722–4727.